Analysis, Circuit Modeling, and Optimization of Mushroom Waveguide Photodetector (Mushroom-WGPD)

Yasser M. El-Batawy, *Student Member, IEEE,* and M. Jamal Deen, *Fellow, IEEE*

***Abstract*—The waveguide photodetector (WGPD) is considered a leading candidate to overcome the bandwidth/quantum-efficiency tradeoff in conventional photodetectors (PDs). To overcome the tradeoff between the capacitance and contact resistance, the mushroom-WGPD was proposed. In this paper, a calibrated circuit model for mushroom-WGPD, including all parasitics, is presented so that a complete circuit simulation of the entire photoreceiver circuit with WGPD now becomes feasible. Both the behavior of the PD and its transfer function for the optical-to-electrical response that can be implemented in a circuit simulator are studied to explore the relationships between performance and design/ material parameters. The effects of the parasitics are also studied for different PD areas. The results from this circuit model of the PD have been compared with a published experimental work and a good agreement is obtained. In addition, the characteristics of mushroom-WGPD are studied for the case of an inductor added in series to the load resistor, and better performance is achieved in comparison to the case with no inductor. Based on the studies of different parameters for design and materials, optimization has been performed for the mushroom-WGPD. With this optimization, the optimal values of the thickness of the absorption layer and the added inductor to produce the highest bandwidth of the PD are obtained. These optimizations are performed for different areas of the PD and also for different load resistors, and they result in a significant improvement in the performance of the mushroom-WGPDs.**

***Index Terms*—Analytical modeling of photodetectors, circuit modeling of photodetectors, modeling of photodiodes, mushroom photodetectors, optimization of photodetectors, parasitics of photodetectors, photodetectors (PDs), photodiodes, waveguide photodetectors.**

I. Introduction

WAVEGUIDE PHOTODETECTORS (WGPDs) are promising high-speed photodetectors (PDs) because both the quantum efficiency as well as the transit-time-limited bandwidth are improved compared with many other photodetector configurations. This improvement is because the light and the carriers are moving in different directions, and hence the bandwidth and the quantum efficiency can be specified almost independently of each other. As the photodetector is illuminated from its side, its quantum efficiency is a function of the length of the absorption layer and not its thickness.

Manuscript received January 15, 2004; revised June 1, 2004. This work was supported in part by the Natural Sciences and Engineering Research Council (NSERC) and Micronet under grants and the Canada Research Chair program.

The authors are with the Electrical and Computer Engineering Department, McMaster University, Hamilton, ON L8S 4K1, Canada (e-mail: ymbatawy@mcmaster.ca; jamal@mcmaster.ca).

Digital Object Identifier 10.1109/JLT.2004.834483

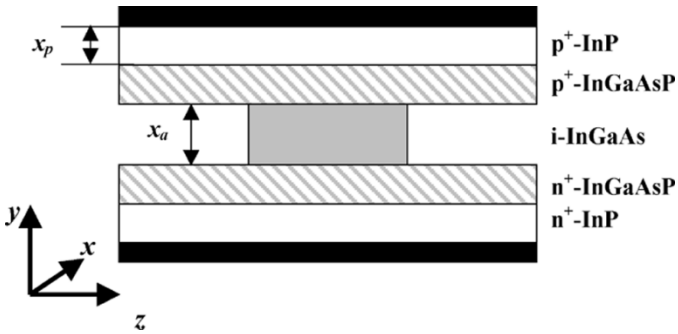

Fig. 1. Schematic representation of a mushroom-WGPD.

Therefore, with a long and thin absorption layer, both high quantum efficiency that depends on the length and low transit time that depends on the thickness can be simultaneously achieved [1]–[9]. An important consideration for these WGPD structures is that due to the small thickness of the absorption layer, the optical coupling with the fiber is sometimes poor, even when a converging lens is used.

Even with the excellent performance in a WGPD, however, there is a tradeoff between the capacitance of the photodetector and its parasitic resistance. It is required to decrease both of them to increase the actual bandwidth of the photodetector. However, a decrease of the area of the photodetector results in a decrease of its capacitance and an increase of its resistance at the same time [10]. The mushroom-WGPD was proposed to overcome the tradeoff between the capacitance and the contact resistance [11]. In [12], a 110-GHz mushroom-WGPD was fabricated. A schematic structure of the mushroom-WGPD is shown in Fig. 1. In this figure, InGaAs is used as the absorption material, and it is lattice-matched to the InP substrate. This combination is suitable for photodetectors for 1.55-μm fiber communication systems. To get rid of the hole-trapping problem, two graded layers of InGaAsP are introduced above and below the absorption layer [13], [14].

This paper is a continuation of our previous work on the modeling of various types of photodetectors [15]–[19]. It presents a circuit model for the mushroom-WGPD, including all its parasitics so that a complete circuit simulation of the entire photoreceiver circuit now becomes feasible. Both the time and the frequency behavior of this photodetector are studied in Section II, for different dimensions of the photodetector, to explore the relationships between performance and design parameters. This study uses the transit-time analysis for conventional p-i-n diodes for a uniform generation that is presented in [20]. In Section III,

the effects of the parasitics on the time behavior of the mushroom-WGPD are studied for different photodetector areas. In addition, the characteristics of mushroom-WGPD are studied for the case of an inductor added in series to the load resistor, and better performance has been achieved in comparison to the case with no inductor. In Section IV, the bandwidth of the photodetector is discussed for different areas and different thicknesses of its absorption layer. In addition, this circuit model is compared with a published experimental work. Based on the studies of different parameters for design and materials, in Section V, optimization is applied for the mushroom-WGPD to get its optimal design. These optimizations are performed for different areas of the photodetector and also for different load resistors, and they result in significant improvement in the performance of the mushroom-WGPDs. Finally, the conclusions are presented in Section VI.

II. Modeling of Mushroom-WGPD

A. Transit Response of Mushroom-WGPD

As the light is incident laterally onto the absorption layer of the photodetector, both electrons and holes are photogenerated and the number of these photogenerated carriers is related to the absorption coefficient of the absorption layer, the dimensions of the photodetector, and the properties of the incident light. Due to the reverse voltage that is applied to the photodetector, the photogenerated electrons move under the effect of the electric field toward the n^+ layer of the photodetector, while the photogenerated holes move toward the p^+ layer. The electric field is assumed to be sufficiently high for the photogenerated carriers to move at their saturation velocities. For this analysis, it is assumed that both the n-layer and the p-layer of the photodetector are heavily doped. Therefore, the photogenerated carriers reach the terminals of the photodetector instantaneously as they enter these layers, and the diffusion of the carriers generated outside the active region into the depletion regions is neglected. In addition, the absorption coefficient of nonactive layers is assumed to be very small compared with that of the active layer so that the generation of carriers outside the active layer can be neglected. Charge trapping is also neglected due to the presence of the grading layers surrounding the absorption layer.

As the light is incident horizontally, the photogeneration rate $g(x)$ will be a function of the horizontal distance x, and it is given by

$$g(x) = g_o \alpha e^{-\alpha x} \delta(t - t_o), \text{ where } g_o = \frac{P_i}{h\nu}. \tag{1}$$

In (1), P_i is the power of the incident light, h is Planck's constant, ν is the frequency of the incident light, α is the effective absorption coefficient of the material of the absorption layer, g_o is the value of the generation rate that depends on the power of the input incident light, δ is the impulse function, t is the time, and t_o is the instant when the light is incident on the photodetector. The absorption coefficient that appears in (1) includes the effect of the confinement factor of the photodetector. In other words, this effective absorption coefficient is expressed as

$$\alpha = \alpha_o \Gamma \tag{2}$$

where Γ is the confinement factor and α_o is the absorption coefficient of the material of the absorption layer. As the photogeneration is in the lateral direction and the movement of the photogenerated carriers is in the perpendicular direction, then photogeneration is uniform and the total photogeneration rate across the absorption layer G is

$$G = \int_0^{L_{\text{core}}} g(x)dx = g_o \left[1 - \exp\left(-\alpha L_{\text{core}}\right)\right] \tag{3}$$

where L_{core} is the length of the absorption layer. Under this uniform photogeneration and for its impulse response, the photogenerated electrons N_{ph} is the sum of the electrons that are traveling to the contact of the photodetector. Then, N_{ph} can be expressed as

$$N_{\text{ph}}(t) = \int_0^{x_a} \frac{G}{x_a} n(x,t)dx, \text{ where } n(x,t) = \begin{cases} 0 & t > \frac{x}{v_n} \\ 1 & t \le \frac{x}{v_n} \end{cases} \tag{4}$$

and the total photogenerated electrons will be

$$N_{\text{ph}}(t) = G\left(1 - \frac{v_n t}{x_a}\right)\left[u(t) - u\left(t - \frac{x_a}{v_n}\right)\right]. \tag{5}$$

Similarly, the total photogenerated holes P_{ph} is

$$P_{\text{ph}}(t) = G\left(1 - \frac{v_p t}{x_a}\right)\left[u(t) - u\left(t - \frac{x_a}{v_p}\right)\right] \tag{6}$$

where v_n and v_p are the saturation velocities for electrons and holes, respectively; x_a is the thickness of the absorption layer; and $u(t)$ is the unit-step time function. The photogenerated current $I_{\text{ph}}(t)$ is given by

$$I_{\text{ph}}(t) = \frac{q}{x_a}\left[v_n N_{\text{ph}}(t) + v_p P_{\text{ph}}(t)\right] \tag{7}$$

where q is the electron charge.

B. Frequency Response of Mushroom-WGPD

The frequency response of mushroom-WGPD is calculated by taking the Fourier transform of the impulse response of the photogenerated electrons and holes that are given by (5) and (6), respectively. The Fourier representations of these photogenerated carriers are given by

$$N_{\text{ph}}(\omega) = G\left(\frac{1}{j\omega} + \frac{v_n\left[1 - \exp\left(-\frac{j\omega x_a}{v_n}\right)\right]}{\omega^2 x_a}\right) \tag{8}$$

and

$$P_{\text{ph}}(\omega) = G\left(\frac{1}{j\omega} + \frac{v_p\left[1 - \exp\left(-\frac{j\omega x_a}{v_p}\right)\right]}{\omega^2 x_a}\right). \tag{9}$$

Using (8) and (9), the photogenerated current in the frequency domain will then be

$$I_{\text{ph}}(\omega) = \frac{q}{x_a}\left(v_n N_{\text{ph}}(\omega) + v_p P_{\text{ph}}(\omega)\right). \tag{10}$$

The current obtained in (10) is called the *intrinsic current* since the effect of the load and the parasitic elements are not considered, so it does not express the actual output current of the photodetector.

C. Circuit Model of Mushroom-WGPD

Fig. 2(a) shows the circuit model of the mushroom-WGPD as the photodetector can be treated as a lumped circuit element. In this model, F is the transfer function of the photodetector. This model is similar to that of the conventional p-i-n photodetector presented in [21] and [22], but it includes a specified transfer function (F) that expresses its response, like that in our previous work in [15] and [16]. In this circuit model, $I_{\rm opt}$ is the optical current that expresses the power of the incident optical pulse, and it is given by

$$I_{\rm opt} = \frac{qP_i}{h\nu}. \tag{11}$$

The transfer function (F) depends on both the material and the thickness of the absorption region. Using (8)–(11), the transfer function of this circuit model is expressed as

$$F(\omega) = \frac{I_{\rm ph}}{I_{\rm opt}} = [1 - \exp(-\alpha L_{\rm core})] \cdot \left(\frac{v_n + v_p}{j\omega x_a} + \frac{v_n^2\left(1-\exp\left(1-\frac{j\omega x_a}{v_n}\right)\right)}{\omega^2 x_a^2} + \frac{v_p^2\left(1-\exp\left(1-\frac{j\omega x_a}{v_p}\right)\right)}{\omega^2 x_a^2} \right). \tag{12}$$

The above transfer function includes only the effects of the photogenerated carriers and not the effects the parasitics that will be described in the next section.

Also in Fig. 2(b), a SPICE presentation of the circuit model of the photodetector is presented. In this representation, a voltage source $V_{\rm opt}$, instead of the optical current source, is included. The transfer function of the photodetector is applied to the FTABLE as a table of magnitude (in decibels) and angle for different frequencies of interest. Then, the output voltage of the FTABLE is transformed to current through the voltage-controlled current source (G) and applied to the load and the parasitic elements to get the frequency response of the photodetector [15], [16].

III. Parasitics Effects of Mushroom-WGPD

The parasitics of the photodetector significantly affect its response, and they are shown in the circuit model in Fig. 2. In this model, C_j is the junction capacitance of the photodetector that is expressed as

$$C_j = \frac{\varepsilon_o \varepsilon_r A_{\rm core}}{x_a} \tag{13}$$

where $A_{\rm core}$ is the area of the absorption layer, and ε_o and ε_r are the free-space permittivity and relative permittivity of the material of the absorption layer, respectively. C_p, which appears in this model, is the pad capacitance, and L_S is the pad inductance

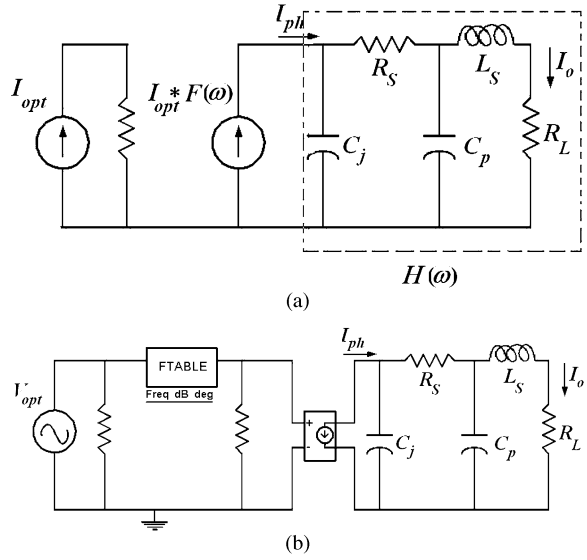

Fig. 2. (a) Circuit model of the mushroom-WGPD. (b) SPICE representation of this model.

or the inductance that may be added in series with the load resistance R_L. R_S is the contact resistance that depends on the doping and the dimension of the p^+ layer, and it is expressed as

$$R_S = \frac{\rho x_p}{A_{\rm PD}} \tag{14}$$

where $A_{\rm PD}$ is the surface area of the p^+ layer, x_p is its thickness, and ρ is the resistivity of its material. In a conventional WGPD, both $A_{\rm PD}$ and $A_{\rm core}$ are the same value, but it differs in the mushroom-WGPD, as the width of the absorption layer is smaller than that of the other layers of the photodetector.

The extrinsic response of the photodetector depends on both the photogenerated carriers and the parasitics elements of the photodetector. Hence, the output extrinsic current of the mushroom-WGPD is expressed as

$$J_{\rm tot}(\omega) = F(\omega) H(\omega) \tag{15}$$

where $H(\omega)$ is the transfer function of the circuit implementation of the parasitics effects of the mushroom-WGPD that are shown in its circuit model. $H(\omega)$ is expressed as

$$H(\omega) = \frac{1}{D(\omega)}$$
$$\text{where } D(\omega) = \left\{ \begin{array}{l} 1 + j\omega\left(C_j\left(R_L + R_s\right) + C_p R_L\right) \\ -\omega^2\left[R_L R_s C_j C_p + L_s\left(C_j + C_p\right)\right] \\ -j\omega^3 L_s R_s C_j C_p \end{array} \right\}. \tag{16}$$

The extrinsic transit response of the photodetector, taking into consideration the effect of the parasitics, will be

$$J_{\rm ext}(t) = F(t) \otimes H(t) \tag{17}$$

where $\otimes$ denotes convolution between the two functions. In the above equation, $H(t)$ is the inverse Laplace transform of $H(\omega)$ that was presented in (16), and it will be

$$H(t) = \mathfrak{L}^{-1}\left\{ \frac{1}{s^2 C_j L_s + s C_j R_{\rm tot} + 1} \right\} \tag{18}$$

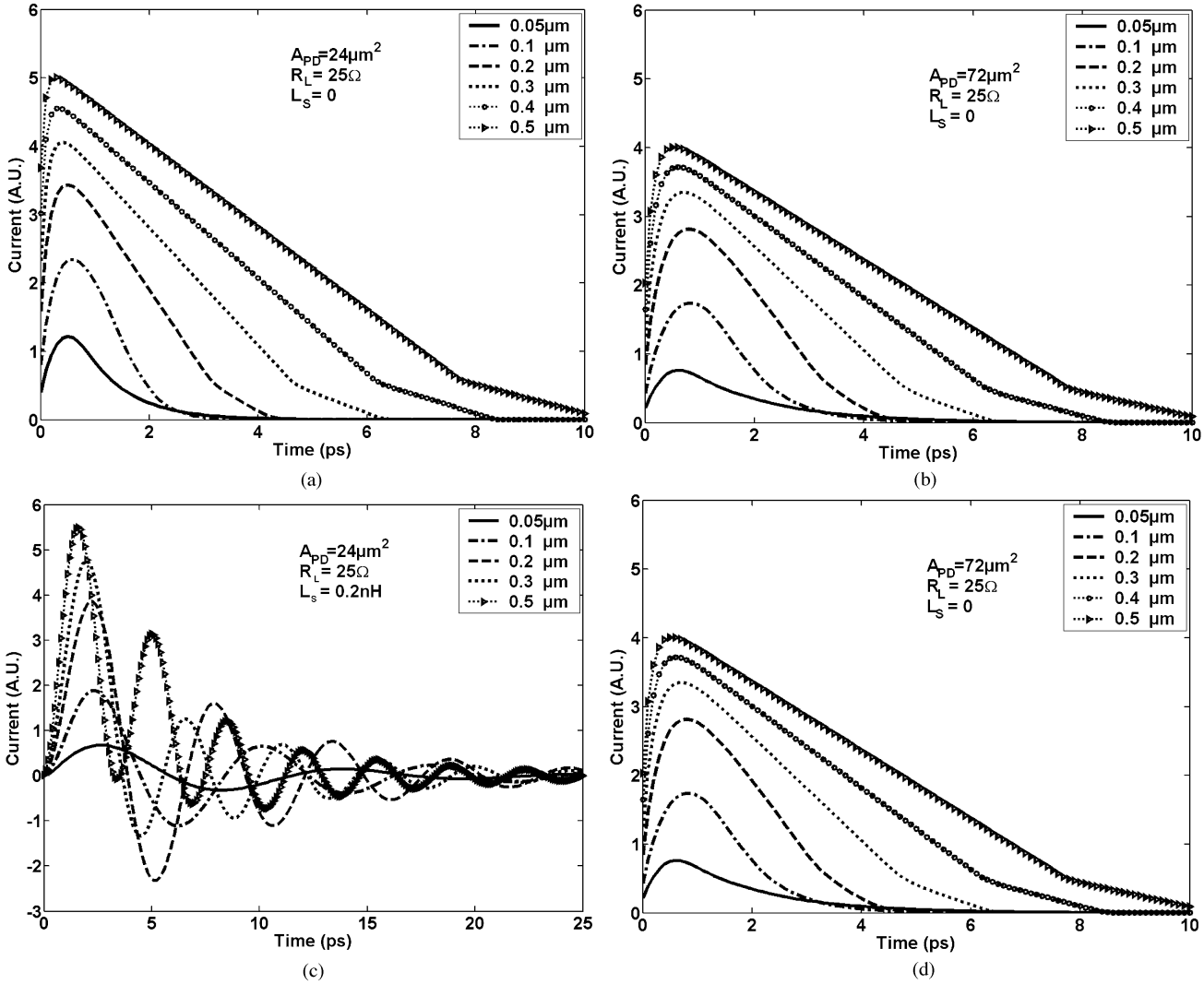

Fig. 3. Transit response of mushroom-WGPD for R_L of 25 Ω for (a) $A_{\rm PD} = 24\ \mu$m^2 and $L_S = 0$, (b) $A_{\rm PD} = 72\ \mu$m^2 and $L_S = 0$, (c) $A_{\rm PD} = 24\ \mu$m^2 and $L_S = 0.2$ nH, and (d) $A_{\rm PD} = 72\ \mu$m^2 and $L_S = 0.2$ nH.

where $s = j\omega$. In the previous equations, the pad capacitance C_p is assumed to be negligibly small and $R_{\rm tot}$ is the summation of both R_L and R_S. If no inductor is connected in series with R_L, then

$$H(t) = \frac{1}{C_j R_{\rm tot}} \exp\left(-\frac{t}{C_j R_{\rm tot}}\right). \tag{19}$$

If an inductor L_s is in series with the load resistance, then there will be two cases depending on its value. The first case is as follows: if $C_d R_{\rm tot}^2 \geq 4L_s$, then

$$H(t) = \frac{1}{\sqrt{\frac{R_{\rm tot}^2}{L_s^2} - \frac{4}{C_j L_s}}} \times \left\{ \exp\left[\left(-\frac{R_{\rm tot}}{2L_s} + \sqrt{\frac{R_{\rm tot}^2}{4L_s^2} - \frac{1}{C_j L_s}}\right) t\right] - \exp\left[\left(-\frac{R_{\rm tot}}{2L_s} - \sqrt{\frac{R_{\rm tot}^2}{4L_s^2} - \frac{1}{C_j L_s}}\right) t\right] \right\}. \tag{20}$$

However, if $C_d R_{\rm tot}^2 < 4L_s$, then

$$H(t) = \frac{1}{\sqrt{C_j L_s - \frac{C_j^2 R_{\rm tot}^2}{4}}} \times \sin\left(t \cdot \sqrt{C_j L_s - \frac{C_j^2 R_{\rm tot}^2}{4}}\right) \exp\left(-\frac{R_{\rm tot}}{2L_s} t\right). \tag{21}$$

The transit response of the mushroom-WGPD is shown in Fig. 3 for different thicknesses of the absorption layer and different areas of the photodetector. This is for an InGaAs absorption layer of width 1.5 μm, while the width of all other layers of the photodetector is 6 μm. As shown in Fig. 3(a) and (b) for photodetector areas $A_{\rm PD}$ of 24 and 72 μm^2, respectively, by increasing the thickness of the absorption layer, the number of the photogenerated carriers increases, and hence the photocurrent increases. However, the distance traveled by the photogenerated carriers increases, resulting in an increase of the transit time taken by the carriers to leave the absorption layer and be collected by the contacts of the photodetector. For a very thin absorption layer and large-area photodetectors, the capacitance

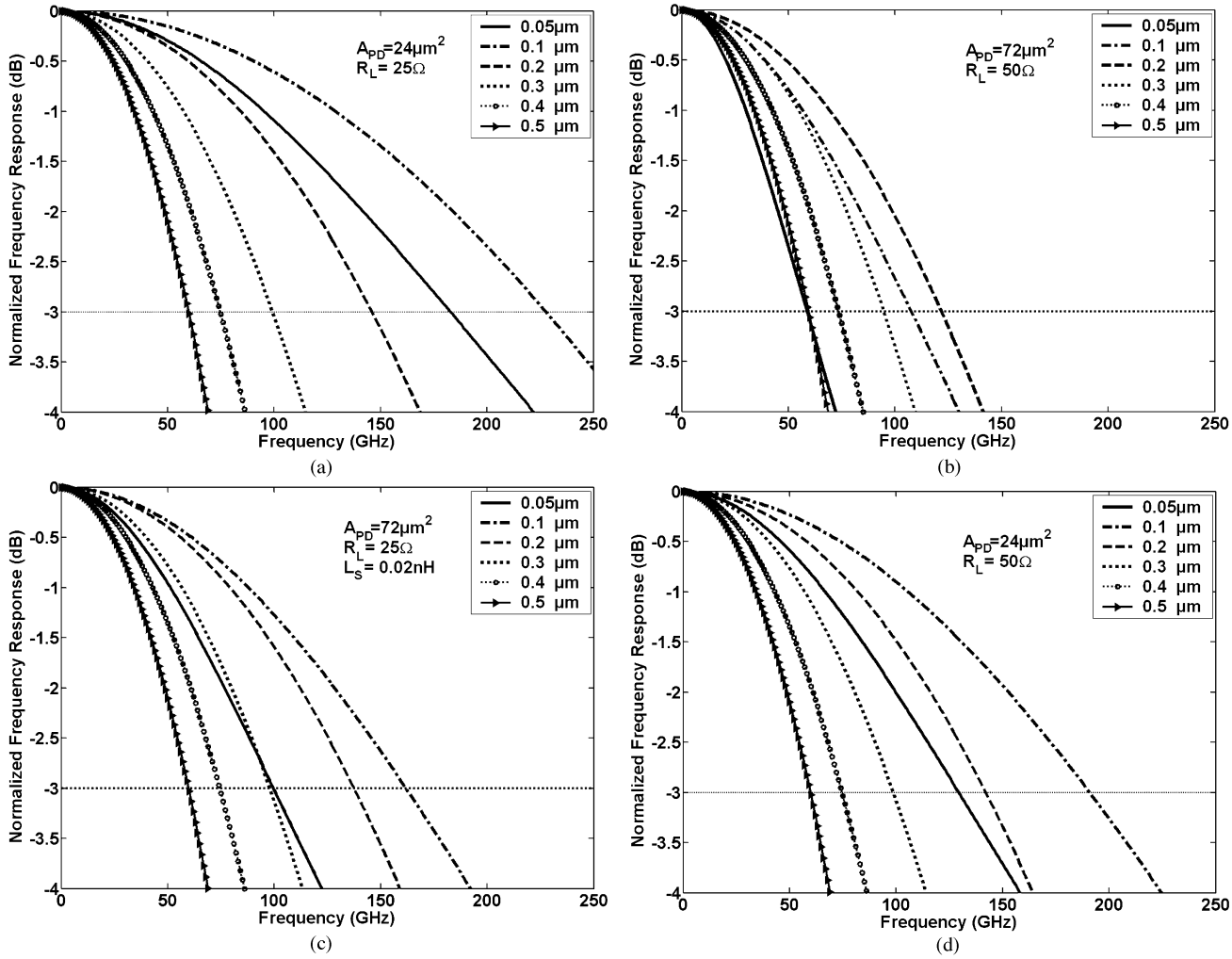

Fig. 4. Frequency response for mushroom-WGPD for (a) Area $= 24\ \mu\text{m}^2$ and $R_L = 25\ \Omega$, (b) Area $= 24\ \mu\text{m}^2$ and $R_L = 50\ \Omega$, (c) Area $= 72\ \mu\text{m}^2$ and $R_L = 25\ \Omega$, and (d) Area $= 72\ \mu\text{m}^2$ and $R_L = 50\ \Omega$.

of the photodetector increases, causing the RC time constant to increase and dominate the transit time of the carriers. The same effect is also observed when the load resistance increases.

Adding an inductor in series with the load resistance results in a decrease of the effect of the capacitance of the photodetector. Peaks will appear in the time response of the photodetector. If the value of this inductor increases, then a sinusoidal effect according to (21) is obtained. This sinusoidal effect appears clearly for large thickness of the absorption layer as the photodetector's capacitance is small for this case, and hence the effect of the inductor on the time response is more clearly seen. This is seen in Fig. 3(c) and (d) where the time behavior of the mushroom-WGPD when a 0.2-nH inductor is added in series with a 25-Ω load resistance is shown. These figures show that the number of peaks of the sinusoidal waveform increases with the thickness of the absorption layer due to the decrease of the photodetector's capacitance. The value of the added inductor should be optimized for different dimensions of the photodetector to get better performance of the photodetector.

IV. Bandwidth of Mushroom-WGPD

In Fig. 4, the normalized frequency response of a mushroom-WGPD for different thicknesses of the absorption layer x_a is presented. The materials used and the related parameter values for this photodetector are presented in Table I. As shown in Fig. 4(a), by decreasing the thickness of x_a, the transit time decreases, and hence the bandwidth of the photodetector increases. For very thin absorption layers, however, the capacitance increases so that the effect of the RC time constant will be the limiting factor for the bandwidth of the photodetector, resulting in a decrease of the bandwidth. Fig. 4(c) shows that by increasing the area of the photodetector, its capacitance increases, resulting in a decrease of the bandwidth. For a large-area photodetector, the RC time constant becomes the limiting factor for the bandwidth, even for thicker absorption layers. As shown in Fig. 4(c) and (d), by increasing the load resistance, the bandwidth of the photodetector decreases due to the increase of the RC time constant of the photodetector. Therefore, optimization should be carried out to get the optimal values of the thicknesses of the absorption layer for different areas and load resistors so that the highest bandwidth can be achieved.

The circuit model that has been described in Sections II and III is compared with the experimental results that are presented in [12]. For a mushroom-WGPD with a 0.2-μm InGaAs absorption layer and with the same material parameters given in Table I, the experimental bandwidth in [12] for this photode-

TABLE I
MATERIALS AND RELATED PARAMETER VALUES OF THE MUSHROOM-WGPD THAT IS USED FOR SIMULATIONS, AND IT IS TYPICAL OF THAT USED IN [12]

Layer and material	Thickness
n InGaAsP	0.8 μm
InGaAs Absorption layer	0.2 μm
p InGaAsP	0.8 μm
p InP	0.5 μm

Parameter	Value
Electron saturation velocity	$6.5\text{x}10^6$ cm/sec
Hole saturation velocity	$4.8\text{x}10^6$ cm/sec
Absorption coefficient	$0.68\text{x}10^4$ cm^{-1}
λ	1.55 μm
ε_r (InGaAs)	14.1

tector is 110 GHz. According to the model that is presented in this paper, the calculated bandwidth is 121 GHz, but this without taking the pad capacitance into consideration. However, if a $C_p = 5$ fF is included, then the calculated bandwidth of the photodetector will be ∼110 GHz.

By including an inductor in series with the load resistance, a compensation of the effect of the capacitance of the photodetector, as described in (16), is obtained, and hence for specific values of this added inductor, the bandwidth of the photodetector can be increased. It is shown in Fig. 5(a) and (b) that by adding a small inductor in series with the load resistance, a small peak appears in the normalized frequency response of the photodetector. There is also an increase in the bandwidth compared with the case of no inductor added in series to the load resistance. Increasing the value of the added inductor results in an increase in the peak of the normalized frequency response, but the bandwidth of the photodetector decreases for some values of the thickness of the absorption layer, as shown in Fig. 5(c). Thus, the value of the added inductor should be optimized to increase the bandwidth of the photodetector, and this optimized inductor depends on the dimensions of the photodetector as well as the value of the load resistance connected to it.

In Fig. 6, the frequency response of mushroom-WGPDs with different widths of the absorption layer is shown. For these WGPDs, the width of the p^+ and n^+ layers is 6 μm. Therefore, if the width of absorption layer is also 6 μm, then it is a conventional WGPD. The performance of the mushroom-WGPD is much better than that of the conventional WGPD, especially for small thicknesses of the absorption layer, as shown in Fig. 6(a) for a 0.1-μm absorption layer and a photodetector area $A_{\rm PD}$ of 24 μm^2. As shown in this figure, by decreasing the width

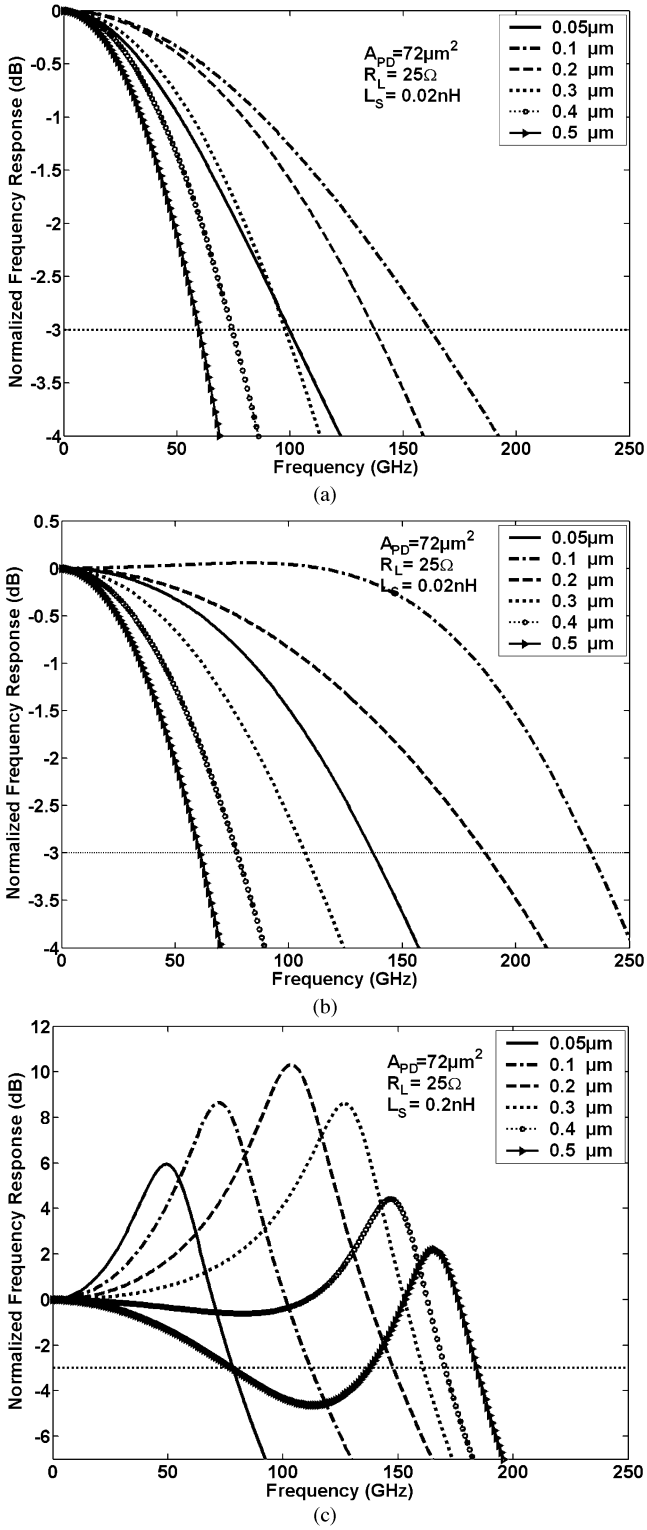

Fig. 5. Frequency response of mushroom-WGPD for $R_L = 25\ \Omega$ and Area $= 72\ \mu\text{m}^2$ for (a) $L_S = 0$, (b) $L_S = 0.02$ nH, and (c) $L_S = 0.2$ nH.

of the absorption layer, an increase of the bandwidth of the photodetector is obtained.

By increasing the area of the photodetector, the bandwidth decreases due to the increase of the capacitance of the photodetector. However, as shown in Fig. 6(b), for a photodetector with area $A_{\rm PD}$ of 72 μm^2, the mushroom-WGPD still has better

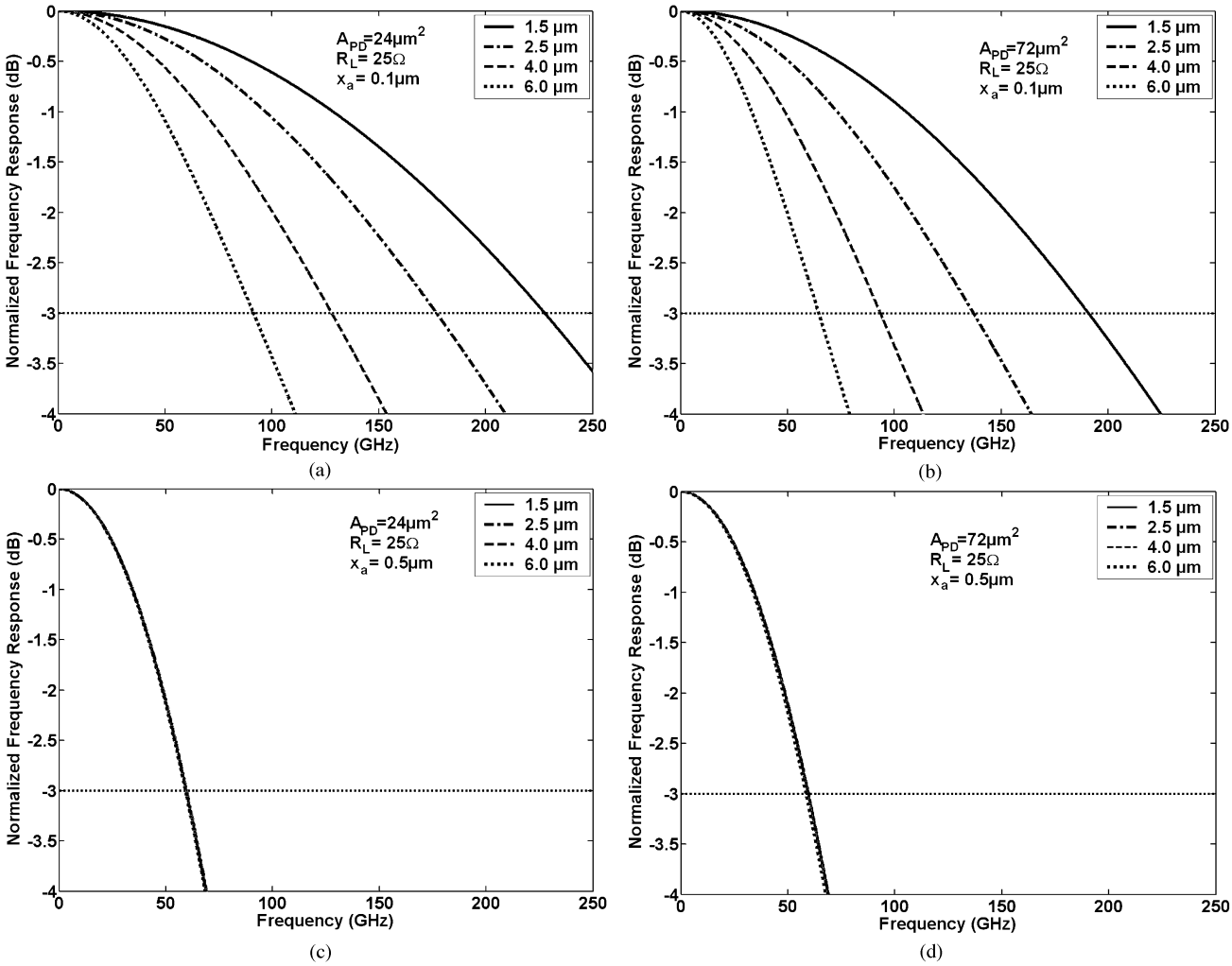

Fig. 6. Frequency response for mushroom-WGPD with different core widths and for a R_L of 25 Ω and for (a) Area $= 24\ \mu\text{m}^2$, $x_a = 0.1\ \mu$m; (b) Area $= 72\ \mu\text{m}^2$, $x_a = 0.1\ \mu$m; (c) Area $= 24\ \mu\text{m}^2$, $x_a = 0.5\ \mu$m; and (d) Area $= 72\ \mu\text{m}^2$, $x_a = 0.5\ \mu$m.

performance than the conventional WGPD. By increasing the thickness of the absorption layer, the performance of mushroom-WGPD and the conventional WGPD are almost the same, as shown in Fig. 6(c) and (d) for a 0.5-μm absorption layer. This is because as the thickness of the absorption layer increases, the bandwidth, which is a transit-time-limited bandwidth, is not affected much by the capacitance of the photodetector. Hence, decreasing the thickness of the core of the WGPD results in almost no advantage in this case.

V. Optimization

Optimization for the bandwidth of the mushroom-WGPD is performed for two cases: the first case when the load is pure resistor and the second case when an inductor is connected in series with the load resistor. In both cases, the optimal thicknesses of the absorption layer are obtained. For the second case, the optimal value of the series inductor is also obtained. The effect of optimization is important since it results in a substantial improvement of the bandwidth of the photodetector.

A. Load Without Inductor

According to (13), for small-area photodetectors, the capacitance decreases. Then, for small-area photodetectors, the optimal value of the thickness of the absorption layer should be small enough to decrease the distance traveled by the photogenerated carriers and hence to decrease the transit time of the photodetector. However, by increasing the area of the photodetector that may be needed for more illumination, the optimal value of the thickness of the absorption layer increases to decrease the capacitance of the photodetector. In Table II, the optimal values of the thickness of the absorption layer of the photodetector and the associated bandwidth are listed for a load resistance of 25 and 50 Ω and for different areas A_{PD} from 24–90 μm^2. As shown in this table, the optimal thickness of the absorption layer are greater for the case of a higher load resistance. This is because for a large load resistance, a lower capacitance is required to increase the photocurrent and to decrease the RC time constant, according to (16).

B. An Inductor in Series With the Load

Optimization for the bandwidth of mushroom-WGPD is performed here to obtain both the optimal thickness of the absorption layer and the optimal L_s to be added in series with the load resistance. These optimizations are done for different photodetector areas that depend on the required value of the photocurrent. The optimal values of L_s and the thickness of the absorp-

TABLE II
OPTIMAL THICKNESS OF THE ABSORPTION LAYER x_a AND THE INDUCTANCE L_S THAT IS ADDED IN SERIES WITH 25- AND 50-Ω LOAD RESISTANCES, AND THE ASSOCIATED BANDWIDTH FOR DIFFERENT AREAS OF THE PHOTODETECTOR

Width (μm)	A_{core} (μm²)	A_{PD} (μm²)	R_L=25Ω					R_L =50Ω				
			Without L_S		With L_S			Without L_S		With L_S		
			$x_{a(Opt)}$ (nm)	BW (GHz)	$x_{a(Opt)}$ (nm)	$L_{S(Opt)}$ (pH)	BW (GHz)	$x_{a(Opt)}$ (nm)	BW (GHz)	$x_{a(Opt)}$ (nm)	$L_{S(Opt)}$ (pH)	BW (GHz)
4	6	24	87.2	231.3	104.7	29.2	348.0	105.4	191.3	126.5	51.5	287.9
6	9	36	96.8	208.5	116.2	26.6	313.7	120.9	166.8	145.5	52.0	250.9
8	12	48	105.4	191.3	126.6	25.8	287.9	134.7	149.8	161.7	53.8	225.4
10	15	60	113.5	177.8	136.3	25.7	267.5	147.1	137.1	176.7	56.1	206.3
12	18	72	120.9	166.8	145.2	26.0	250.9	158.6	127.2	190.9	58.7	191.3
15	22	90	131.4	153.5	157.8	26.6	231.0	174.4	115.6	209.9	62.6	174.0

tion layer of mushroom-WGPD with the photodetector's area $A_{\rm PD}$ from 24–90 μm^2 for load resistances of 25 and 50 Ω are listed in Table II. A shown in this table, for the optimal values of the parameters of the photodetector, the bandwidth increases significantly compared with the case of a pure load resistance.

All the previous optimizations for mushroom-WGPD have been done for InGaAs absorption layer material that is matched to the InP substrate, and this combination is suitable for the detection of incident light of a wavelength of 1.55 μm [12]. All these optimization techniques can also be applied to other material combination for different-wavelength photodetectors.

VI. CONCLUSION

In this paper, first, a circuit model of the mushroom-WGPD was presented where the photodetector is treated as a lumped circuit element. The transfer function of this model and the effects of the photodetector's parameters on it have been studied. The circuit model can be generalized for other types of WGPDs. The effects of the thicknesses of the absorption layers of the photodetector on the transfer function of this circuit model were discussed. Prediction with this circuit model is in good agreement with a published experimental result.

The effects of area and the width of the core of the photodetector on its bandwidth were investigated. Adding an inductance in series with the load resistance results in an improvement of its bandwidth. Optimization was applied to the photodetector to get the optimal thickness of the absorption layer for different areas of the photodetector. This has been done for two cases: first for a pure load resistance and second for an inductor connected in series with the load resistor. The optimal value of the inductor in the second case was also obtained. This small inductor that is in series with the load resistor results in a significant improvement of the bandwidth of the photodetector. Optimizations were also performed for different values of the load resistor and also for different areas of the photodetector, resulting in significant improvement in the mushroom-WGPD's performance. For a larger load resistor, the optimal value of the thickness of the absorption layer of the photodetector increases. In addition, by increasing the area of the photodetector, the optimal value of this thickness increases.

REFERENCES

[1] K. Kato and Y. Akatsu, "High-speed waveguide photodetectors," in *Proc. 7th Int. Conf. InP Related Materials*, May 1995, pp. 349–352.

[2] A. Bandyopadhy and M. J. Deen, "Photodetector for optical fiber communications," in *Photodetectors and Fiber Optics*, H. S. Nalwa, Ed. NewYork: Academic, 2001, pp. 307–368.

[3] K. Kato, S. Halta, A. Kozen, J. Yoshida, and K. Kawano, "High efficiency waveguide InGaAs PIN photodiode with bandwidth of over 40 GHz," *IEEE Photon. Technol. Lett.*, vol. 3, no. 6, pp. 473–474, Jun. 1991.

[4] D. Wake, T. P. Spooner, S. D. Perrin, and M. J. Harlow, "50 GHz InGaAs edge-coupled PIN photodetector," *Electron. Lett.*, vol. 27, pp. 1073–1075, Jun. 1991.

[5] A. Umbach, M. Leone, and G. Unterbörsch, "High-frequency behavior of waveguide integrated photodiodes monolithically integrated on InP using optical butt coupling," *J. Appl. Phys.*, vol. 81, pp. 2511–2516, Mar. 1997.

[6] K. Kato, "Ultrawide-band/high-frequency photodetectors," *IEEE Trans. Microwave Theory Tech.*, vol. 47, no. 7, pp. 1265–1281, Jul. 1999.

[7] S. D. McDougall, M. J. Jubber, O. P. Kowalski, J. H. Marsh, and J. S. Aitchison, "GaAs/AlGaAs waveguide pin photodiodes with nonabsorbing input facets fabricated by quantum well intermixing," *Electron. Lett.*, vol. 36, pp. 749–750, Apr. 2000.

[8] G. S. Kinsey, C. C. Hansing, A. L. Holmes Jr., B. G. Streetman, J. C. Campbell, and A. G. Dentai, "Waveguide $\rm In_{0.53}Ga_{0.47}As$-$\rm In_{0.52}Al_{0.48}As$ avalanche photodiode," *IEEE Photon. Technol. Lett.*, vol. 12, no. 4, pp. 416–418, Apr. 2000.

[9] N. R. Das, Y. M. El-Batawy, and M. J. Deen, "Optoelectronic integrated circuit photoreceivers for fiber-optic telecommunication," in *Proc. 1st Int. Symp. Integrated Optoelectronics, Electrochemical Society*, vol. PV2002–4, May 2002, pp. 163–194.

[10] K. Kato, S. Hata, K. Kawano, J. Yoshida, and A. Kozen, "A high-efficiency 50 GHz InGaAs multimode waveguide photodetector," *IEEE J. Quantum Electron.*, vol. 28, no. 12, pp. 2728–2735, Dec. 1992.

[11] K. Kato and J. Yoshida, "Ultrawide-bandwidth 1.55 μm waveguide p-i-n photodiode," in *Proc. SPIE—Int. Soc. Optical Engineering*, vol. 2149, 1994, pp. 312–319.

[12] K. Kato, A. Kozen, Y. Muramoto, Y. Itaya, T. Nagatsuma, and M. Yatia, "110-GHz, 50%-efficiency mushroom-mesa waveguide p-i-n photodiode for a 1.55-μm wavelength," *IEEE Photon. Technol. Lett.*, vol. 6, no. 6, pp. 719–721, Jun. 1994.

[13] K. A. Anselm, H. Nie, C. Lenox, P. Yuan, G. Kinsey, J. C. Campbell, and B. G. Streetman, "Performance of thin separate absorption, charge, and multiplication avalanche photodiodes," *IEEE J. Quantum Electron.*, vol. 34, no. 3, pp. 482–490, Mar. 1998.

[14] H. Nie, O. Baklenov, P. Yuan, C. Lenox, B. G. Streetman, and J. C. Campbell, "Quantum-dot resonant-cavity separate absorption, charge and multiplication avalanche photodiodes operating at 1.06 μm," *IEEE Photon. Technol. Lett.*, vol. 10, no. 7, pp. 1009–1011, Jul. 1998.

[15] Y. M. El-Batawy and M. J. Deen, "Modeling and optimization of resonant cavity enhanced-separated absorption graded charge multiplication-avalanche photodetector (RCE-SAGCM-APD)," *IEEE Trans. Electron Devices*, vol. 50, no. 3, pp. 790–801, Mar. 2003.

[16] Y. M. El-Batawy, M. J. Deen, and N. R. Das, "Analysis, optimization and SPICE modeling of resonant cavity enhanced PIN photodetector," *J. Lightw. Technol.*, vol. 22, no. 9, pp. 2031–2043, Sep. 2003.
[17] Y. M. El-Batawy and M. J. Deen, "Modeling of mushroom waveguide photodetector (mushroom-WGPD)," J. Vac. Sci. Technol., vol. 22, pp. 811–815, May 2004, to be published.
[18] Y. G. Xiao and M. J. Deen, "Theoretical approach to frequency response of resonant-cavity avalanche photodiodes," in *Proc. SPIE, Photodetectors: Materials Devices VI*, vol. 4288, Jn. 2001, pp. 21–30.
[19] ——, "Frequency response and modeling of resonant-cavity separate absorption, charge and multiplication avalanche photodiodes," *J. Lightw. Technol.*, vol. 19, no. 7, pp. 1010–1022, Jul. 2001.
[20] G. Lucovsky, R. F. Schwarz, and R. B. Emmons, "Transit-time considerations in p-i-n diodes," *J. Appl. Phys.*, vol. 35, no. 3, pp. 622–628, Mar. 1964.
[21] D. Huber, R. Bauknecht, C. Bergamaschi, M. Bitter, A. Huber, T. Morf, A. Neiger, M. Rohner, I. Schnyder, V. Schwarz, and H. Jäckel, "InP–InGaAs single HBT technology for photoreceiver OEIC's at 40 Gb/s and beyond," *J. Lightw. Technol.*, vol. 18, no. 7, pp. 992–998, Jul. 2000.
[22] K. Yang, A. L. Gutierrez-Aitken, X. Zhang, G. I. Haddad, and P. Bhattacharya, "Design, modeling, and characterization of monolithically integrated InP-based (1.55 μm) high-speed (24 Gb/s) p-i-n/HBT front-end photoreceivers," *J. Lightw. Technol.*, vol. 14, no. 8, pp. 1831–1839, Aug. 1996.

Yasser M. El-Batawy (S'04) was born in Cairo, Egypt, in 1973. He received the B.Sc. degree in electrical communications and electronics and the M.Sc. degree in engineering physics from Cairo University, Cairo, Egypt, in 1996 and 2000, respectively. Since 2001, he has been working toward the Ph.D. degree with the Department of Electrical and Computer Engineering, McMaster University, Hamilton, ON, Canada, where he is working on theory, modeling, characterization, simulation, and optimization of high-speed photodetectors.

He was a Research and Teaching Assistant in the Department of Engineering Physics, Cairo University, from 1996 to 2000. He is currently working on theory, modeling, characterization, simulation, and optimization of high-speed photodetectors.

Mr. El-Batawy was the recipient of the 2002–2003, 2003–2004, and 2004–2005 Ontario Graduate Scholarship (OGS).

M. Jamal Deen (S'81–M'82–SM'92–F'03) was born in Georgetown, Guyana. He received the B.Sc. degree in physics and mathematics from the University of Guyana, Turkeyen, Guyana, in 1978 and the M.S. degree and the Ph.D. degree in electrical engineering and applied physics from Case Western Reserve University (CWRU), Cleveland, OH, in 1982 and 1985, respectively.

He was a Research Engineer (1983–1985) and an Assistant Professor (1985–1986) with Lehigh University, Bethlehem, PA. In 1986, he joined the School of Engineering Science, Simon Fraser University, Vancouver, BC, Canada, as an Assistant Professor, and from 1993 to 2002, he was a Full Professor. In summer 1999, he assumed his current position as Professor of Electrical and Computer Engineering, McMaster University, Hamilton, ON, Canada. He was awarded a Senior Canada Research Chair in Information Technology in July 2001. He was a Visiting Scientist at the Herzberg Institute of Astrophysics, National Research Council, Ottawa, ON, Canada, in summer 1986, and he spent his sabbatical leave as a Visiting Scientist at Northern Telecom, Ottawa, ON, Canada, from 1992 to 1993. He was a Visiting Professor in the Faculty of Electrical Engineering, Delft University of Technology in summer 1997, and a CNRS Directeur de Recherche at the Physics of Semiconductor Devices Laboratory, Grenoble, France, in summer 1998 and the Universiti de Montpellier, Montpellier, France, in 2002–2003. He has edited two research monographs and eight conference proceedings. He has written 14 invited book chapters, was awarded six patents, has published more that 300 peer-reviewed articles, and has given more than 60 invited/keynote conference presentations. His current research interests include physics, modeling, reliability and parameter extraction of semiconductor devices; optical detectors and receivers; and low-power, low-noise, and high-frequency circuits.

Dr. Deen is a Member of Eta Kappa Nu, the American Physical Society, and the Electrochemical Society. He was a Fulbright-Laspau Scholar from 1980 to 1982, an American Vacuum Society Scholar from 1983 to 1984, and an NSERC Senior Industrial Fellow in 1993. He is a Distinguished Lecturer of the IEEE Electron Devices Society (EDS); was awarded the 2002 Thomas D. Callinan Award from the Electrochemical Society—Dielectric Science and Technology Division; and the Distinguished Researcher Award, Province of Ontario, in July 2001. He is currently an Editor of IEEE TRANSACTIONS ON ELECTRON DEVICES; Executive Editor of *Fluctuations and Noise Letters;* and Member of the Editorial Board of *Interface*, an Electrochemical Society journal.